

Article

## Enhanced Microwave Absorption Properties of $\alpha$ -Fe<sub>2</sub>O<sub>3</sub>-Filled Ordered Mesoporous Carbon Nanorods

Yiming Wang, Liuding Wang and Hongjing Wu \*

Department of Applied Physics, School of Science, Northwestern Polytechnical University, Xi'an 710072, China; E-Mails: wym2010@mail.nwpu.edu.cn (Y.W.); wangld@nwpu.edu.cn (L.W.)

\* Author to whom correspondence should be addressed; E-Mail: wuhongjing@mail.nwpu.edu.cn; Tel.: +86-29-8843-1664; Fax: +86-29-8843-1664.

Received: 15 March 2013; in revised form: 3 April 2013 / Accepted: 7 April 2013 /

Published: 15 April 2013

---

**Abstract:** A novel kind of  $\alpha$ -Fe<sub>2</sub>O<sub>3</sub>-filled ordered mesoporous carbon nanorods has been synthesized by a facial hydrothermal method. Compared with dendritic  $\alpha$ -Fe<sub>2</sub>O<sub>3</sub> micropines, both a broader effective absorption range—from 10.5 GHz to 16.5 GHz with reflection loss (RL) less than  $-10$  dB—and a thinner matching thickness of 2.0 mm have been achieved in the frequency range 2–18 GHz. The enhanced microwave absorption properties evaluated by the RL are attributed to the enhanced dielectric loss resulting from the intrinsic physical properties and special structures.

**Keywords:** ordered mesoporous carbon;  $\alpha$ -Fe<sub>2</sub>O<sub>3</sub>; dielectric loss; microwave absorption

---

### 1. Introduction

In recent years, the study of microwave absorbing materials has attracted much attention for electromagnetic interference (EMI) shielding and electromagnetic (EM) wave absorbing applications, for both commercial and defense purposes [1–3]. Traditional spinel-type ferrites have been extensively studied, however they have some disadvantages such as low permeability, caused by Snoek's limit, and large density hinder their further development [4]. On the other hand, dielectric absorbers have potential as microwave absorbents due to advantages such as low density, controllable dielectric loss ability, and so on [5]. However, compared with ferrite materials, dielectric fillers such as carbon fiber and multi-walled carbon nanotubes are used to control complex permittivity only [6]. The complex permeability and permittivity of dielectric dissipation materials are out of balance, and their impedance

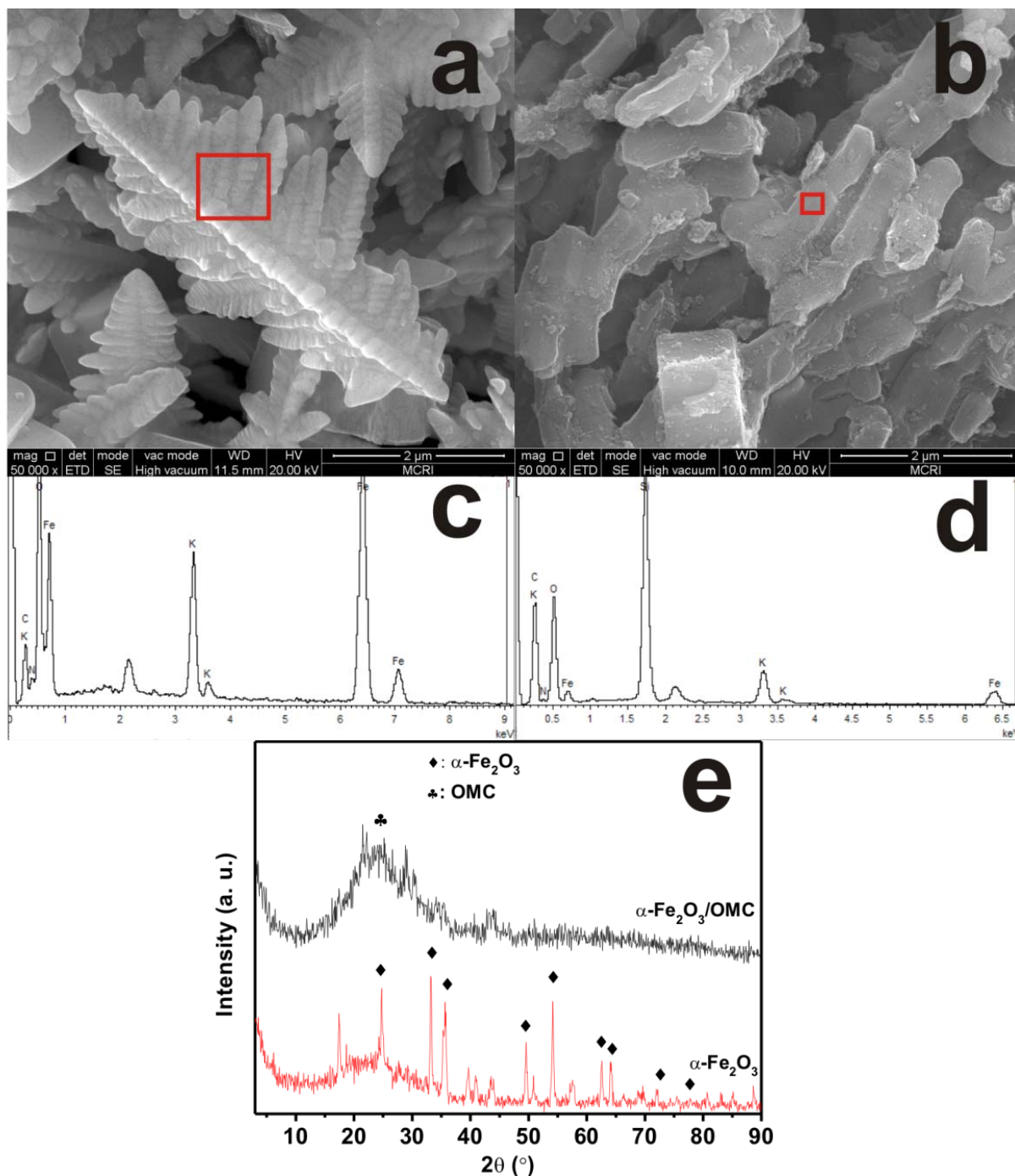
matching characteristic is poor [7]. Recently, many studies have been carried out to investigate the complementary behavior of magnetic or dielectric microwave absorber coatings by mixing multi-walled carbon nanotubes or metallic magnetic materials [8,9]. Several groups have reported excellent microwave absorption properties of heterogeneously structured nanocomposites, such as  $\text{Fe}_3\text{O}_4$ -poly(3,4-ethylenedioxythiophene) (PEDOT) microspheres [10], hierarchical magnetic yolk/shell microspheres [11], nanocomposites, *etc.* These heterogeneous structures exhibit interesting chemistry as well as effective interfaces and material-dependent properties, endowing such structures with enhanced properties, or satisfactory synergistic effects for microwave absorption enhancement. However, up until now very little attention has been directed toward the magnetic particle-filled ordered mesoporous carbon materials for microwave absorption applications.

The purpose of this study was to investigate the electromagnetic and microwave absorption properties of hybrid nanorods consisting of ordered, mesoporous carbon (OMC) and  $\alpha\text{-Fe}_2\text{O}_3$ , which may adjust the dielectric properties of  $\alpha\text{-Fe}_2\text{O}_3$  and OMC and contribute to the microwave absorption properties. Most interestingly, it exhibited a broader absorption bandwidth and lighter weight in the studied range of 2–18 GHz than the as-synthesized dendritic  $\alpha\text{-Fe}_2\text{O}_3$  micro-pines. It was found that a multi-loss combination in the unique  $\alpha\text{-Fe}_2\text{O}_3$ /OMC hybrid structures contributed to enhanced microwave absorption.

## 2. Results and Discussion

Representative SEM images of the as-synthesized products are shown in Figure 1a,b respectively. It can be clearly seen that dendritic  $\text{Fe}_2\text{O}_3$  micropines can be formed by using a facial hydrothermal reaction at low temperatures [12]. As shown in Figure 1a, the high magnification image of a single dendrite shows a hierarchical structure with tertiary branches. The lengths of the dendrite trunks are 3–5  $\mu\text{m}$ , and those of the branch trunk range from 50 nm to 1  $\mu\text{m}$ , which is very consistent with the report of Sun *et al.* [12]. When OMC is added to the solution of 0.1 mol  $\text{L}^{-1}$   $\text{K}_3[\text{Fe}(\text{CN})_6]$  in a Teflon-sealed autoclave,  $\text{Fe}_2\text{O}_3$ -filled OMC structures are obtained, as shown in Figure 1b. Compared with the electron microscopy of undoped OMC [13], it is found that the  $\text{Fe}_2\text{O}_3$ -filled OMC structures are relatively thick, suggesting that  $\text{Fe}_2\text{O}_3$  nanoparticles are mostly embedded in the carbon walls of OMC. Figures 1c,d show the main peaks of O, Fe, and C elements in the energy dispersive spectroscopy (EDS) spectrum, indicating that the nanorods contain a  $\text{Fe}_2\text{O}_3$  component. Figure 1e shows the XRD pattern of the dendritic  $\text{Fe}_2\text{O}_3$  micropines, in which all diffraction peaks indicated by Miller indices can be indexed to  $\alpha\text{-Fe}_2\text{O}_3$ . There are also peaks which are not well defined. These peaks may be assigned to the intermediate products when preparing dendritic  $\text{Fe}_2\text{O}_3$  micropines, which would not contribute to the absorption properties of the composites. It suggests that  $\alpha\text{-Fe}_2\text{O}_3$  dendrites are highly crystalline. However, the  $\alpha\text{-Fe}_2\text{O}_3$ -filled OMC nanocomposites are relatively amorphous, exhibiting weak diffraction peaks for  $\alpha\text{-Fe}_2\text{O}_3$  in the XRD pattern, expect for a diffraction hump of carbon around 15°–35°.

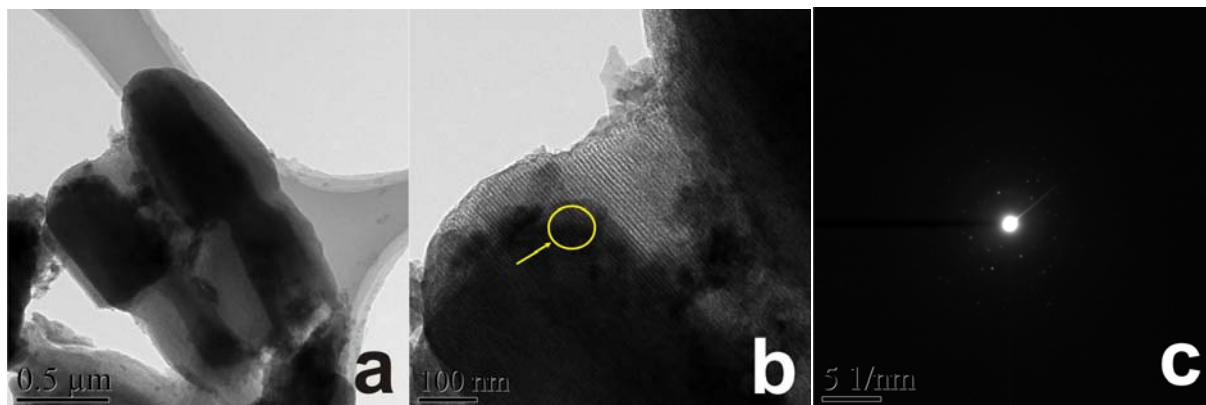
**Figure 1.** Structural characterizations of dendritic  $\alpha$ -Fe<sub>2</sub>O<sub>3</sub> micropines and  $\alpha$ -Fe<sub>2</sub>O<sub>3</sub>/OMC nanorods: (a,b) scanning electron microscope (SEM) images; (c,d) energy dispersive spectroscopy (EDS) spectrum; and (e) X-ray diffraction on a diffractometer (XRD) patterns.



The morphology of as-prepared  $\alpha$ -Fe<sub>2</sub>O<sub>3</sub>/OMC hybrid structure was investigated in detail by TEM, and shown in Figure 2. Figure 2a shows a low magnification TEM micrograph of  $\alpha$ -Fe<sub>2</sub>O<sub>3</sub>/OMC hybrid nanorods, in which all the nanorods seem to have a core-shell structure. However, the  $\alpha$ -Fe<sub>2</sub>O<sub>3</sub> core regime is formed by filling the mesopores of OMC with  $\alpha$ -Fe<sub>2</sub>O<sub>3</sub> nanoparticles. The formation of the OMC shell may have been caused by not completely filling the  $\alpha$ -Fe<sub>2</sub>O<sub>3</sub> nanoparticles. Strictly, it is not really a core-shell structure. As shown in Figure 2b, the  $\alpha$ -Fe<sub>2</sub>O<sub>3</sub> appears black and OMC is light

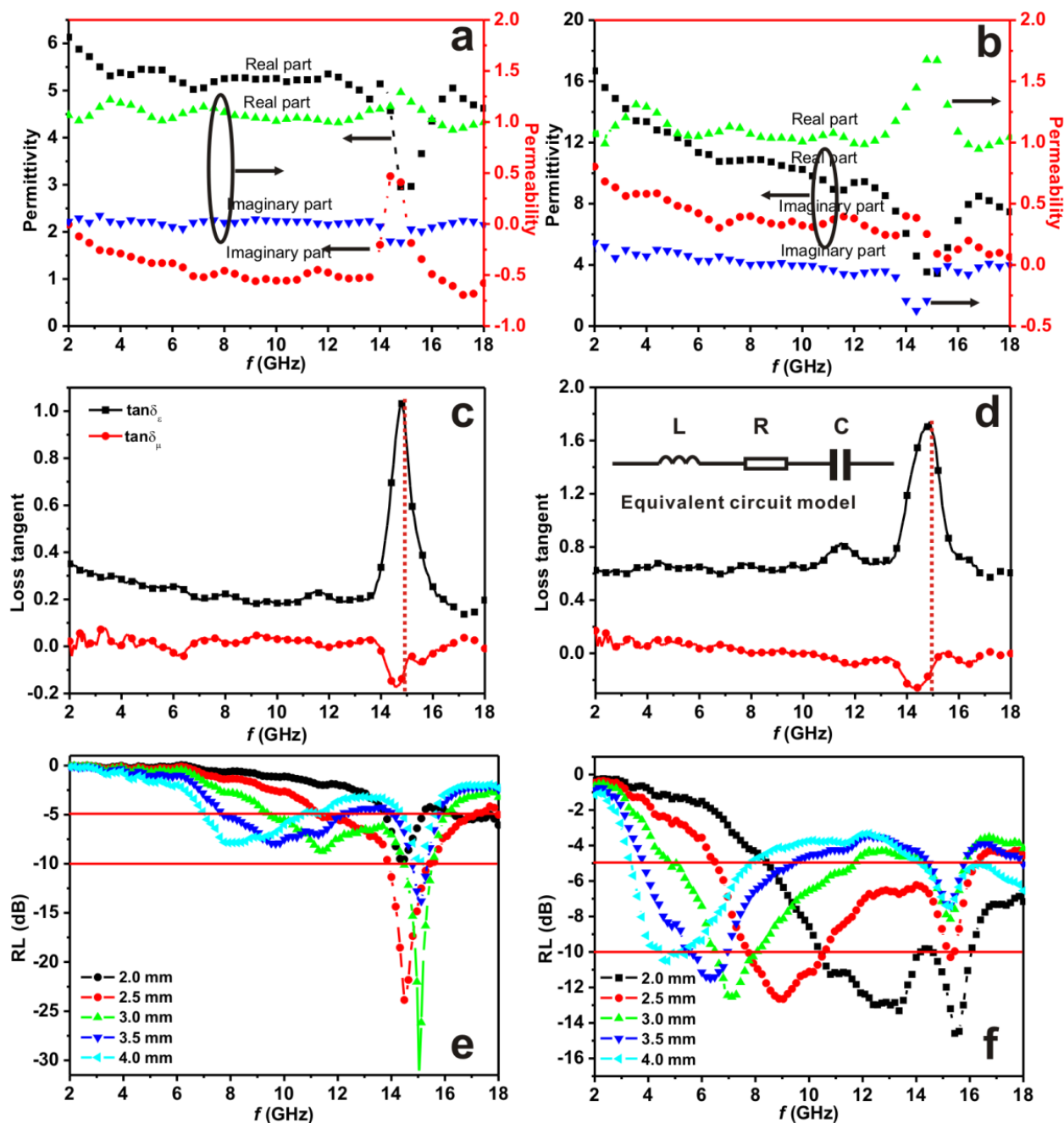
colored in the image, because hematite has a higher mass–thickness contrast. The bright dot patterns from SAED of the sample given in Figure 2c can be well-indexed to the crystalline phase of hematite.

**Figure 2.** (a,b) transmission electron microscope (TEM) images and (c) SAED of  $\alpha$ -Fe<sub>2</sub>O<sub>3</sub>/OMC nanorods.



The electromagnetic (EM) parameters (relative complex permittivity,  $\varepsilon = \varepsilon' - j\varepsilon''$  and relative complex permeability,  $\mu_r = \mu' - j\mu''$ ) of the wax composites containing 50 wt % of the as-synthesized samples were measured at room temperature. Figure 3a,b show the measured  $\varepsilon_r$  and  $\mu_r$  in the range of 2–18 GHz for the two samples. The  $\varepsilon'$  and  $\varepsilon''$  values of  $\alpha$ -Fe<sub>2</sub>O<sub>3</sub> microdendrites are in the range 3–6 and 0.5–3 over a frequency region of 2–18 GHz. However, those values are much lower than those of  $\alpha$ -Fe<sub>2</sub>O<sub>3</sub>/OMC hybrid nanorods (4–17 for  $\varepsilon'$  and 4.5–11.5 for  $\varepsilon''$ ). It suggests that  $\alpha$ -Fe<sub>2</sub>O<sub>3</sub>/OMC hybrid nanorods have a strong dielectric loss when exposed to EM waves. The dielectric loss tangent ( $\tan \delta_e = \varepsilon''/\varepsilon'$ ) of the two samples is shown in Figure 3c,d. The  $\tan \delta_e$  values of  $\alpha$ -Fe<sub>2</sub>O<sub>3</sub>/OMC hybrid nanorods larger than 0.6 are distributed between 2 and 18 GHz and exhibit a peak value of 1.7 at 15 GHz, whereas the values for  $\alpha$ -Fe<sub>2</sub>O<sub>3</sub> microdendrites are in the range 0.2–0.4 over the frequency range 2–14 GHz, indicating a strong dielectric resonance at the high frequency range in the case of  $\alpha$ -Fe<sub>2</sub>O<sub>3</sub>/OMC hybrid nanorods. In general, high dielectric loss results from the inherent physical properties of OMC and their special heterogeneous structures. Ordered mesoporous carbon (OMC) materials have large surface areas, so the number of surface atoms with unsaturated bonds is greatly increased, resulting in an increase of dipoles. Consequently, the dipole polarizations could contribute to dielectric loss. Furthermore the microstructure of  $\alpha$ -Fe<sub>2</sub>O<sub>3</sub> nanoparticles filling a carbon matrix would provide additional interfaces around the nanoparticles, and the interfacial polarization associated with relaxation could give rise to dielectric loss as well. The above two dielectric loss aspects can be confirmed by the *Cole-Cole* semicircle, as shown in Figures 2S(a) and 2S(b) [13–15], because the *Cole-Cole* semicircle is a typical feature of dielectric relaxation. In addition, because of the addition of the conductive material OMC, the increase in electric conductivity of the  $\alpha$ -Fe<sub>2</sub>O<sub>3</sub>/OMC hybrid nanorods results in an enhanced conductance loss, as shown in Figures 2S(a) and 2S(b) (red dashed lines) [16,17].

**Figure 3.** (a,b) relative complex permittivity and permeability; (c,d) dielectric and magnetic tangent loss; (e,f) reflection loss of  $\alpha$ -Fe<sub>2</sub>O<sub>3</sub> microdendrites and  $\alpha$ -Fe<sub>2</sub>O<sub>3</sub>/OMC nanorods respectively. The inset in Figure 3d is a *LRC* equivalent circuit model.



The  $\mu'$  and  $\mu''$  values of the two samples (Figure 3a,b) indicate that  $\mu'$  is close to one, while the  $\mu''$  is almost equal to zero in the frequency range 2–18 GHz, except for a resonant frequency at around 15 GHz. Moreover, the  $\mu''$  value is negative at this resonant frequency. Considerable attempts have been made to obtain an exact solution of the phenomenon that causes the values of permeability  $\mu''$  to be negative at some frequencies. Chiu [18] has pointed out that it is meaningless and may be due to noise, although we have previously explained the phenomenon as the outward radiation of magnetic energy, resulting in a conversion of the incident wave to other forms of energy [13–15]. So, in the present work we consider that this phenomenon may be related to the eddy currents on the surface of

$\alpha$ -Fe<sub>2</sub>O<sub>3</sub>/OMC structures and  $\alpha$ -Fe<sub>2</sub>O<sub>3</sub> dendrites which can produce an induced magnetic field, and in turn radiate EM waves, leading to an increase in the total magnetic energy and hence a negative  $\mu''$  in the measured frequency range [15]. According to the references [13–15], if the values of  $\mu''(\mu')^{-2}f^{-1}$  is kept constant while the frequency is varied, the magnetic loss only results from eddy current loss. From Figures 2S(c) and 2S(d) it can be found that an eddy current may occur on the surface of  $\alpha$ -Fe<sub>2</sub>O<sub>3</sub>/OMC composites. The magnetic loss tangent ( $\tan \delta_m = \mu''/\mu'$ ) of the two samples is simply the inverse to that of  $\tan \delta_e$ , as shown in Figure 3c,d, which can be explained by the LRC equivalent circuit model (see the inset in Figure 3d), where  $L$ ,  $R$ , and  $C$  are the inductance, resistance and capacitance respectively. In particular, the eddy current effect regarded as inductance, the dielectric relaxation polarization playing a role as capacitance, and the conductance loss acted as resistance all contribute to the LRC equivalent circuit model. The inverse change trend is attributed to the capacitance leading or lagging behind the inductance by an angle of 90° [15].

On the basis of transmission line theory [19] the reflection loss (RL) can be calculated; the results are shown in Figure 3e,f. It can be seen clearly that the  $\alpha$ -Fe<sub>2</sub>O<sub>3</sub>/OMC hybrid nanorods with a coating layer thickness of 2.0 mm exhibit a broader absorption bandwidth than the  $\alpha$ -Fe<sub>2</sub>O<sub>3</sub> microdendrites, corresponding to an RL below -10 dB with the same thickness, which can reach up to 6.0 GHz (from 10.5 GHz to 16.5 GHz). It is also noted that the absorption peak value of  $\alpha$ -Fe<sub>2</sub>O<sub>3</sub> microdendrites is much higher than that of the  $\alpha$ -Fe<sub>2</sub>O<sub>3</sub>/OMC hybrid nanorods, but its absorption bandwidth is too narrow to be widely applied. Figure 4a,b show the color map of the reflection loss values calculated from the measured EM parameters of nanocomposites. It is obvious that for  $\alpha$ -Fe<sub>2</sub>O<sub>3</sub>/OMC hybrid nanorods, RL exceeds -10 dB in the range of 4–18 GHz for absorber thicknesses of 1.5–5.0 mm. Compared with the recent representative nanocomposites, the as-synthesized  $\alpha$ -Fe<sub>2</sub>O<sub>3</sub>/OMC hybrid nanorods present a similar microwave absorption performance with thin thickness and broad absorption range, as shown in Table 1. However, we report a novel synthetic approach that can be used to prepare magnetic particle-filled ordered mesoporous carbon materials for microwave absorption application. The enhanced microwave properties of the  $\alpha$ -Fe<sub>2</sub>O<sub>3</sub>/OMC hybrid nanorods are attributed to a major dielectric loss and a minor eddy current loss, leading to the microwave absorption enhancement.

**Figure 4.** Reflection loss map of (a)  $\alpha$ -Fe<sub>2</sub>O<sub>3</sub> microdendrites and (b)  $\alpha$ -Fe<sub>2</sub>O<sub>3</sub>/OMC nanorods.

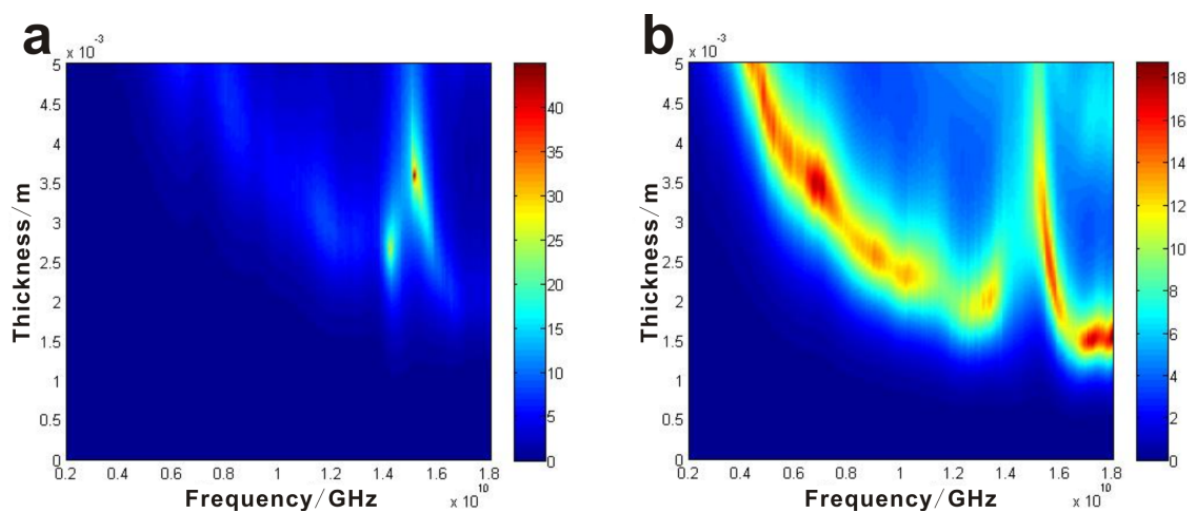


**Table 1.** Microwave absorption performance of some representative nanocomposites.

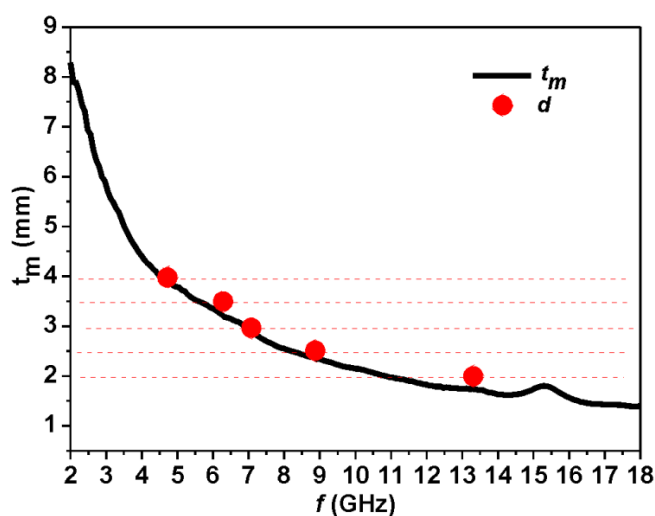
Samples	Minimum RL value (dB)	Frequency range (GHz) (RL < -10 dB)	$d_m$ (mm) (RL < -10 dB)	Percentage (wt % or vol %)	References
Fe <sub>3</sub> O <sub>4</sub> /PEDOT	-30	~8–13	4 mm	20 (vol %)	[10]
Porous Fe <sub>3</sub> O <sub>4</sub> /carbon	-27.9	~13–18	2 mm	55 (wt %)	[16]
$\alpha$ -Fe <sub>2</sub> O <sub>3</sub>	-23.9	13.8–15.5	2.5 mm	50 (wt %)	this work
$\alpha$ -Fe <sub>2</sub> O <sub>3</sub> /OMC	-15.0	10.5–16.5	2 mm	50 (wt %)	this work

Besides the major dielectric loss, electromagnetic waves could be absorbed via a so-called “geometrical effect” [17]. The “geometrical effect” means that when the thickness of absorber ( $t_m$ ) satisfies the following Equation (1), the reflected waves are totally canceled in the air-absorber interface:

$$t_m = \frac{n\lambda_m}{4}, \left( n = 1, 3, 5, \dots; \lambda_m = \frac{\lambda_0}{\sqrt{|\epsilon_r \mu_r|}}; \lambda_0 = \frac{c}{f_m} \right) \quad (1)$$

where  $\lambda_m$  is the wavelength in the absorber at some specific frequency,  $f_m$ ;  $|\epsilon_r|$  and  $|\mu_r|$  are the moduli of  $\epsilon_r$  and  $\mu_r$ , respectively; and  $\lambda_0$  is the wavelength in free space. The calculated frequency dependence of  $t_m$  is shown in Figure 5 (black line) for the  $\alpha$ -Fe<sub>2</sub>O<sub>3</sub>/OMC hybrid nanorods sample. The thickness (denoted as  $d$ )—corresponding to the minimum RL in Figure 4f—is also plotted in Figure 5 with red circles. The calculated thickness  $t_m$  is consistent with  $d$ , which implies that the corresponding  $f_m$  and the matching thickness  $d$  is coincident with the quarter wavelength matching condition. Therefore, the above calculations justify that the selective absorption properties of the  $\alpha$ -Fe<sub>2</sub>O<sub>3</sub>/OMC hybrid nanorods at certain frequencies is due to the geometric effect.

**Figure 5.** The frequency dependence of matching thickness  $d$  and calculated thickness  $t_m$  for  $\alpha$ -Fe<sub>2</sub>O<sub>3</sub>/OMC hybrid nanorods.



### 3. Experimental Section

#### 3.1. Materials

The synthesis of mesoporous silica (*i.e.*, SBA-15) was prepared using the triblock copolymer, EO<sub>20</sub>PO<sub>70</sub>EO<sub>20</sub> (Pluronic P123, BASF) as the surfactant and tetraethylorthosilicate (TEOS, 98%, Acros, Japan) as the silica source. Raw commercial HCl, H<sub>2</sub>SO<sub>4</sub>, NaOH, K<sub>3</sub>[Fe(CN)<sub>6</sub>], and sucrose as the carbon source were purchased from Sinopharm Chemical Reagent Co. Ltd., China.

#### 3.2. Sample Preparation

In this work, OMC was synthesized by using mesoporous silica SBA-15 as a hard template, as reported in our previous works [13–15]. One-dimensional (1-D)  $\alpha$ -Fe<sub>2</sub>O<sub>3</sub>/OMC hybrid nanorods were synthesized by a facile hydrothermal method in a 100 mL autoclave at 140 °C for 48 h and masses of 3.29 g for K<sub>3</sub>[Fe(CN)<sub>6</sub>] and 0.50 g for OMC were chosen. For comparison, dendritic  $\alpha$ -Fe<sub>2</sub>O<sub>3</sub> micropines were fabricated by the same method, except for the addition of OMC. Then the resulting compounds were filtrated, washed and dried in air at 80 °C overnight. The paraffin wax composites were prepared by ultrasonic agitation to mix a certain weight fraction (50 wt %) of absorbent with paraffin wax matrix.

#### 3.3. Measurements

The as-prepared samples were characterized by X-ray diffraction on a diffractometer (XRD; D/MAX, Rigaku, Japan), scanning electron microscope (SEM; JSM-5610LV, JEOL, Japan), energy-dispersive X-ray spectroscopy (EDS; OXFORD INCA, UK), and transmission electron microscope (TEM; JEM-3010, JEOL, Japan). The as-prepared paraffin wax composites were pressed into a toroid with an outer diameter of 7.0 mm, inner diameter of 3.04 mm, and thickness of 3.0 mm. The scattering parameters of the toroidal samples (S<sub>11</sub>, S<sub>21</sub>) were measured by bidirectional transmission/reflection method in a coaxial measurement fixture (as shown in Figure 1S) with the HP 8720B network analyzer over 2–18 GHz. The electromagnetic parameters—relative complex permittivity,  $\epsilon_r = \epsilon' - j\epsilon''$  and relative complex permeability,  $\mu_r = \mu' - j\mu''$ —were determined by the complex scattering parameters using the Nicolson–Ross model [20,21]. The reflection loss (RL) was calculated using the following equations [19]:

$$Z_{in} = Z_0(\mu_r / \epsilon_r)^{1/2} \tanh[j(2\pi fd/c)(\mu_r \epsilon_r)^{1/2}], \quad RL = 20 \log |(Z_{in} - Z_0) / (Z_{in} + Z_0)| \quad (2)$$

where  $\mu_r$  and  $\epsilon_r$  are the relative permeability and permittivity,  $f$  is the frequency of the electromagnetic wave,  $d$  is the thickness of the absorber,  $c$  is the velocity of light,  $Z_0$  is the impedance of free space, and  $Z_{in}$  is the input impedance of the absorber.

### 4. Conclusions

In summary, one dimensional (1D)  $\alpha$ -Fe<sub>2</sub>O<sub>3</sub>/OMC hybrid nanorods have been fabricated by the facial hydrothermal method. The unique heterogeneous structure of  $\alpha$ -Fe<sub>2</sub>O<sub>3</sub>/OMC hybrid nanorods greatly enhance the dielectric loss of the materials, and therefore not only a broader effective



absorption range from 10.5 GHz to 16.5 GHz with reflection loss less than  $-10$  dB, but also a lighter weight and thinner matching thickness (2.0 mm) have been achieved. Combining the complementarities with intrinsic physical properties and special structures, the hybrid nanorods can be used as a promising EM wave absorber.

### Acknowledgments

This project was financially supported by the National Natural Science Foundation of China (No. 50771082 and No. 60776822), the Excellent Doctorate Foundation, Doctorate Foundation (CX201207) and Graduate Starting Seed Fund (Z2011011) of Northwestern Polytechnical University, and the Scholarship Award for Excellent Doctoral Student granted by Ministry of Education.

### References

1. Vinoy, K.J.; Jha, R.M. *Radar Absorbing Materials from Theory to Design and Characterization*; Kluwer Academic Publishers: Boston, MA, USA, 1996.
2. Tsutaoka, T.; Ueshima, M.; Tohunaga, T. Frequency dispersion and temperature variation of complex permeability of Ni–Zn ferrite composite materials. *J. Appl. Phys.* **1995**, *78*, 3983–3991.
3. Saib, A.; Vanhoenacker-Janvier, D.; Huynen, I.; Encinas, A.; Piraux, L.; Ferain, E.; Legras, R. Magnetic photonic band-gap material at microwave frequencies based on ferromagnetic nanowires. *Appl. Phys. Lett.* **2003**, *83*, 2378–2380.
4. Smit, J.; Wijn, H.P.J. *Ferrites*; Philips Technical Library: Eindhoven, the Netherlands, 1959.
5. Xu, H.L.; Bi, H.; Yang, R.B. Enhanced microwave absorption property of bowl-like  $\text{Fe}_3\text{O}_4$  hollow spheres/reduced graphene oxide composites. *J. Appl. Phys.* **2012**, *111*, 07A522:1–07A522:3.
6. Tellakula, R.A.; Varadan, V.K.; Shami, T.C.; Mathur, G.N. Carbon fiber and nanotube based composites with polypyrrole fabric as electromagnetic absorbers. *Smart Mater. Struct.* **2004**, *13*, 1040–1044.
7. Park, K.Y.; Lee, S.E.; Kim, C.G.; Han, J.H. Application of MWNT-added glass fabric/epoxy composites to electromagnetic wave shielding enclosures. *Compos. Struct.* **2007**, *81*, 401–406.
8. Qing, Y.C.; Zhou, W.C.; Luo, F.; Zhu, D.M. Epoxy-silicone filled with multi-walled carbon nanotubes and carbonyl iron particles as a microwave absorber. *Carbon* **2010**, *48*, 4074–4080.
9. Zhou, J.H.; He, J.P.; Li, G.X.; Wang, T.; Sun, D.; Ding, X.C.; Zhao, J.Q.; Wu, S.C. Direct incorporation of magnetic constituents within ordered mesoporous carbon-silica nanocomposites for highly efficient electromagnetic wave absorbers. *J. Phys. Chem. C* **2010**, *114*, 7611–7617.
10. Zhou, W.C.; Hu, X.J.; Bai, X.X.; Zhou, S.Y.; Sun, C.H.; Yan, J.; Chen, P. Synthesis and electromagnetic, microwave absorbing properties of core-shell  $\text{Fe}_3\text{O}_4$ -poly(3,4-ethylenedioxythiophene) microspheres. *ACS Appl. Mater. Interfaces* **2011**, *3*, 3839–3845.
11. Liu, J.W.; Xu, J.J.; Che, R.C.; Chen, H.J.; Liu, Z.W.; Xia, F. Hierarchical magnetic yolk-shell microspheres with mixed barium silicate and barium titanium oxide shells for microwave absorption enhancement. *J. Mater. Chem.* **2012**, *22*, 9277–9284.
12. Sun, G.B.; Dong, B.X.; Cao, M.H.; Wei, B.Q.; Hu, C.W. Hierarchical dendrite-like magnetic materials of  $\text{Fe}_3\text{O}_4$ ,  $\gamma\text{-Fe}_2\text{O}_3$ , and Fe with high performance of microwave absorption. *Chem. Mater.* **2011**, *23*, 1587–1593.

13. Wu, H.J.; Wang, L.D.; Guo, S.L.; Wang, Y.M.; Shen, Z.Y. Electromagnetic and microwave-absorbing properties of highly ordered mesoporous carbon supported by gold nanoparticles. *Mater. Chem. Phys.* **2012**, *133*, 965–970.
14. Wu, H.J.; Wang, L.D.; Wang, Y.M.; Guo, S.L.; Shen, Z.Y. Enhanced microwave absorbing properties of carbonyl iron-doped Ag/ordered mesoporous carbon nanocomposites. *Mater. Sci. Eng. B* **2012**, *177*, 476–482.
15. Wu, H.J.; Wang, L.D.; Wang, Y.M.; Guo, S.L.; Shen, Z.Y. Enhanced microwave performance of highly ordered mesoporous carbon coated by Ni<sub>2</sub>O<sub>3</sub> nanoparticles. *J. Alloys Compd.* **2012**, *525*, 82–86.
16. Chen, Y.J.; Xin, G.; Wang, T.S.; Ouyang, Q.Y.; Qi, L.H.; Ma, Y.; Gao, P.; Zhu, C.L.; Cao, M.S.; Jin, H.B. Porous Fe<sub>3</sub>O<sub>4</sub>/carbon core/shell nanorods: Synthesis and electromagnetic Properties. *J. Phys. Chem. C* **2011**, *115*, 13603–13608.
17. Deng, L.J.; Han, M.G. Microwave absorbing performances of multiwalled carbon nanotube composites with negative permeability. *Appl. Phys. Lett.* **2007**, *91*, 023119:1–023119:3.
18. Chiu, S.C.; Yu, H.C.; Li, Y.Y. High electromagnetic wave absorption performance of silicon carbide nanowires in the gigahertz range. *J. Phys. Chem. C* **2010**, *114*, 1947–1952.
19. Naito, Y.; Suetake, K. Application of ferrite to electromagnetic wave absorber and its characteristics. *IEEE Trans. Microw. Theory Tech.* **1971**, *19*, 65–72.
20. Nicolson, A.M.; Ross, G.F. Measurement of the intrinsic properties of materials by time-domain techniques. *IEEE Trans. Instrum. Meas.* **1970**, *19*, 377–382.
21. Yusoff, A.N.; Abdullah, M.H.; Ahmad, S.H.; Jusoh, S.F.; Mansor, A.A.; Hamid, S.A.A. Electromagnetic and absorption properties of some microwave absorbers. *J. Appl. Phys.* **2002**, *92*, 876–882.

© 2013 by the authors; licensee MDPI, Basel, Switzerland. This article is an open access article distributed under the terms and conditions of the Creative Commons Attribution license (<http://creativecommons.org/licenses/by/3.0/>).